

Title:

Radio frequency electromagnetic field compliance assessment of multi-band and MIMO equipped radio base stations

Authors:

Björn Thors, Ericsson Research, SE-164 80 Stockholm, Sweden

bjorn.thors@ericsson.com, +46 10 717 18 24 (corresponding author)

Arno Thielens, Department of Information Technology, Ghent University/iMinds,
9000 Gent, Belgium

Jonas Fridén, Ericsson Research, SE-417 56 Gothenburg, Sweden

Davide Colombi, Ericsson Research, SE-164 80 Stockholm, Sweden

Christer Törnevik, Ericsson Research, SE-164 80 Stockholm, Sweden

Günter Vermeeren, Department of Information Technology, Ghent University/iMinds,
9000 Gent, Belgium

Luc Martens, Department of Information Technology, Ghent University/iMinds,
9000 Gent, Belgium

Wout Joseph, Department of Information Technology, Ghent University/iMinds,
9000 Gent, Belgium

Running title:

RF EMF compliance assessments of RBS

Abstract

In this paper, different methods for practical numerical radio frequency (RF) exposure compliance assessments of radio base station (RBS) products are investigated. Both multi-band base station antennas and antennas designed for multiple-input multiple-output (MIMO) transmission schemes are considered. For the multi-band case, various standardized assessment methods are evaluated in terms of resulting compliance distance with respect to the International Commission on Non-Ionizing Radiation Protection (ICNIRP) reference levels and basic restrictions. Both single frequency and multiple frequency (cumulative) compliance distances are determined, using numerical simulations for a mobile communication base station antenna transmitting in four frequency bands between 800 MHz and 2600 MHz. The assessments are conducted in terms of the root-mean squared electromagnetic field, the whole-body averaged SAR and the peak 10g averaged SAR. In general, assessments based on peak field strengths are found to be less computationally intensive but lead to larger compliance distances than spatial averaging of electromagnetic fields used in combination with localized SAR assessments. As long as adult exposure is considered, the results also indicate that even shorter compliance distances are obtained by using assessments based on localized and whole-body SAR. Numerical simulations, using base station products employing multiple-input multiple-output (MIMO) transmission schemes, are performed as well and are in good agreement with reference measurements. The applicability of various field combination methods for correlated exposure is investigated, and best estimate methods are proposed. It is also shown, that field combining methods generally considered as conservative may be used to efficiently assess compliance boundary dimensions of single- and dual-polarized multicolumn base station antennas with only minor increases in compliance distances.

Key words: Mobile communication; Electromagnetic field exposure; EMF compliance; Specific Absorption Rate; MIMO; Multi-standard radio base station; Multi-band radio base station.

INTRODUCTION

Before radio base station (RBS) products are placed on the market, their manufacturers conduct electromagnetic field (EMF) product compliance assessments to make sure that the equipment fulfills relevant regulatory requirements on EMF exposure. The purpose of these assessments is to determine compliance boundaries outside of which the radiofrequency (RF) EMF exposure is below applicable exposure limits. The most widely adopted exposure limits are specified by the International Commission on Non-Ionizing Radiation Protection (ICNIRP) [ICNIRP, 1998]. For frequencies between 10 MHz to 10 GHz, including the frequency range used for mobile communications, the fundamental dosimetric quantity is the specific absorption rate (SAR). SAR corresponds to the rate of dissipated energy per unit mass within the exposed body due to the incident electromagnetic fields. Assessing exposure with respect to the basic restrictions either requires expensive measurement systems or advanced numerical simulations. For practical exposure assessments, ICNIRP specifies another set of limits denoted reference levels. The reference levels, given in terms of electric and magnetic field strengths and power density, are to be assessed in free space. They are derived from the basic restrictions using numerical modeling and laboratory investigations [ICNIRP, 1998].

Numerical simulation procedures for EMF product compliance assessments of RBSs are standardized in Europe by the European Committee for Electrotechnical Standardization (CENELEC) [CENELEC, 2010] and globally by the International Electrotechnical Commission (IEC) [IEC, 2011]. These standards contain general specifications, with limited guidance on practical issues related to modeling and simulations of RBS antennas. In the literature, numerical SAR assessments have been reported in a number of studies using various techniques [Cooper et al., 2002; Joseph et al., 2003; Joseph and Martens, 2005; Martínez-Búrdalo et al., 2005; van Wyk et al., 2005; Kos et al., 2011]. Results from numerical SAR simulations, evaluated against the basic restrictions, have also been compared with power density results, evaluated with respect to the reference levels [Dimbylow, 2002; Lacroux et al., 2008; Thielens et al., 2013]. In most of these studies, either simple generic or detailed antenna models are used. For the detailed antenna models, replication of the fine geometrical structures of the corresponding physical

antennas produces results of high accuracy. A disadvantage, however, is that the creation of the numerical antenna model can be time-consuming. For numerical product compliance assessments, it is essential that the procedure employed results in an accurate and efficient modeling of the real-world antenna. Furthermore, in the reported studies, different types of anatomical human phantom models have been used. Since SAR depends on the size and shape of the considered phantoms, the obtained results may only be valid for a subset of the human population. For product compliance tests on the other hand, it is important that the assessments are conducted using standardized procedures to obtain repeatable results with a quantified uncertainty.

Modern RBS products are multi-standard and support several radio access technologies to allow more flexible and cost-effective network deployments. If multi-band antennas are used with these products, the combined exposure from the individual sources has to be considered.

Another trend in telecommunications is the rapid increase of data traffic in the networks due to the growth of mobile broadband usage. To enhance system performance and service capabilities, multiple input multiple output (MIMO) transmission schemes, employed together with multiple antennas at the transmitter and receiver, can be used [Dahlman et al., 2008]. Here, the sources are transmitting in the same frequency band, and the electromagnetic fields may be either correlated or uncorrelated depending on the used MIMO scheme. RF exposure compliance methodologies for MIMO enabled networks are reported by Pernetos et al. [2012], which studied the impact of field correlation and various field combining methods for a scenario with two vertically polarized base station antennas horizontally separated by 10 wavelengths. Note that other antenna realizations, with the antenna columns placed close together, also are possible. An accurate exposure assessment of multicolumn array antennas requires that the mutual coupling between the antenna columns is considered.

In this paper, various aspects related to practical numerical RF EMF compliance assessments of radio base station products are investigated. Assessments are made for typical mobile communication frequencies using standardized, and in some cases non-standardized, procedures based on peak electromagnetic fields, spatially averaged electromagnetic fields, peak 10g averaged SAR and whole-

body averaged SAR [CENELEC, 2010; IEC, 2011]. The objective is twofold. Firstly, to compare for the first time, different RF exposure assessment methods based on the different aforementioned quantities in order to select an efficient, yet conservative, assessment of compliance boundaries. Secondly, to compare different numerical algorithms for radio base stations employing MIMO transmission schemes in order to provide guidance on how the choice of method impacts the accuracy of the compliance boundary dimensions. These numerically determined compliance boundaries, based on peak electromagnetic fields, are validated with measurements.

MATERIALS AND METHOD

Field combining near radio base stations for uncorrelated and correlated exposure

When assessing exposure from multiple electromagnetic sources the different contributions have to be combined. In this context, it is important to first determine whether the fields at the point of investigation shall be regarded as correlated or uncorrelated [IEC, 2010].

The fields are uncorrelated if different data streams are being transmitted or if the signals are transmitted at different carrier frequencies. This applies for the multi-band antennas considered in this paper. For uncorrelated sources transmitting at mobile communication frequencies, the combined exposure is readily assessed by summation of exposure ratios in terms of SAR, power density, or squared electric and magnetic fields, depending on the exposure metric considered [ICNIRP, 1998]. As an example, the total exposure ratio (ER) of a multiband or multiport antenna can be written as:

$$ER(\mathbf{r}) = \sum_{n=1}^N \max \left(\frac{|w_n \mathbf{E}_n(\mathbf{r})|_{\text{rms}}^2}{E_{\text{lim}}(f_n)^2}, \frac{|w_n \mathbf{H}_n(\mathbf{r})|_{\text{rms}}^2}{H_{\text{lim}}(f_n)^2} \right), \quad (1)$$

where the summation is taken over all frequency bands and antenna ports (N). Here, w_n , f_n , \mathbf{E}_n , and \mathbf{H}_n denote the complex excitation coefficients associated with port/band n , the frequency at port/band n , and the corresponding electric and magnetic fields at assessment point \mathbf{r} when only port n is excited with $w_n = 1$. The subscript rms indicates root-mean-squared. $E_{\text{lim}}(f_n)$ and $H_{\text{lim}}(f_n)$ denote the frequency dependent rms reference levels for the electric and magnetic fields at frequency f_n ,

respectively. Compliance with the exposure limits at the assessment point \mathbf{r} is obtained if $ER(\mathbf{r})$ is below one.

In the following, equations are only given for the electric field to simplify the notation. Expressions for the magnetic field may be stated analogously and it is understood that all comparisons against exposure limits are made by forming exposure ratios considering both the electric and magnetic fields as in (1).

For correlated exposure, which is of relevance for the MIMO case, the combined electric field strength can be written as the sum of the true vector fields. The RF exposure is to be time-averaged over six minutes when compared with the ICNIRP limits. In practice, the excitation coefficients will in most cases vary over a much shorter time frame [Dahlman et al., 2008]. This variation depends on the traffic and radio conditions. Furthermore, the amplitude and/or the phase of the inputs to the antenna ports (w_n) may be known only with a limited accuracy. Therefore, a straightforward summation of the true vector fields is unpractical. For the MIMO assessments, a conservative approach is instead adopted where the fields are assumed to be correlated, and the exposure is maximized for every evaluation point according to the field combining method considered. This implies that for every evaluation point a specific array excitation $\mathbf{w} = (w_1, \dots, w_N)$ is used. Even though this resulting field distribution is not physically realizable, the approach is justified by the objective to determine a compliance boundary. The approach has the advantage that knowledge of the exact excitations \mathbf{w} is not needed, which simplifies the exposure assessment. In this paper, field combining for two cases is analyzed. In the first case, the amplitude distribution of the excitation is fixed and known (for a given total transmitted power) but the phase ϕ may vary arbitrarily. In the second case, the excitations \mathbf{w} vary in both amplitude and phase for a fixed transmitted power.

Fixed Amplitude distribution, varying phases. For the first case, three different field combining methods are considered [IEC, 2010]:

$$\left\{ \begin{array}{l} E_{\text{rms}}(\mathbf{r}) \leq \sum_{n=1}^N |w_n| |E_n(\mathbf{r})|_{\text{rms}} \quad (\text{Magnitude method}) \quad (2) \\ E_{\text{rms}}(\mathbf{r}) \leq \sqrt{\sum_{\tau=x,y,z} \left(\sum_{n=1}^N |w_n| |E_{n,\tau}(\mathbf{r})|_{\text{rms}} \right)^2} \quad (\text{Components method}) \quad (3) \\ E_{\text{rms}}(\mathbf{r}) = \max_k \left| \sum_{n=1}^N |w_n| e^{j\varphi_{n,k}} E_n(\mathbf{r}) \right|_{\text{rms}}, \quad k = 1, 2, \dots, N_\varphi \quad (\text{Random Phase method}) \quad (4) \end{array} \right.$$

Here, $\varphi_{n,k}$ denotes the k^{th} phase excitation of port n and N_φ the number of random phases considered per field evaluation point in the Random Phase method. The first two methods (denoted ‘‘Magnitude method’’ and ‘‘Components Method’’) yield upper bounds of the true vector field sum. For the Magnitude method, equality between the left and right hand is obtained for situations where the fields have the same polarization and are temporally in phase, whereas for the Components method, equality between the left and right hand is obtained for situations where the fields are in phase temporally [IEC, 2010]. Theoretically, Equation (3) provides a lower degree of overestimation compared with Equation (2), but the obtained combined electric field is in general not invariant under coordinate transformations [Perentos, 2012]. For the Random Phase method, a set of random phases is created for each field evaluation point. The phase excitations resulting in the largest combined field strengths are retained and the resulting combined fields are stored. The total number of phases processed per field evaluation point N_φ is given by

$$N_\varphi = N_p^{N-1} + 1. \quad (5)$$

Here, N_p denotes the number of phases per port (port 2 to N) and the additional phase (+1) corresponds to a uniform phase excitation. The latter is always included to maximize the field strength for evaluation points located along the beam pointing direction of the unsteered antenna. In contrast to the conservative field combining methods in Equations (2) and (3), the Random Phase method in Equation (4) should, after convergence, provide a best estimate approximation of the realistic compliance boundary dimensions.

The Magnitude method is significantly faster than the Random Phase method, but for assessments of MIMO antennas transmitting with different nominal polarizations a straightforward application of the Magnitude method will lead to a significant overestimation of the front compliance distance, because the fields associated with ports of different antenna polarization will be orthogonal in this direction. As a consequence, the Magnitude method is unsuitable for this case. The total field corresponding to contributions from antenna ports with the same nominal polarization can, however, be well approximated using the Magnitude method. These combined fields (for different nominal polarizations) may then be subsequently combined using power summation according to Equation (1). Based on this observation the following approach is proposed, which below is referred to as the X-pol Magnitude method: (i) Columns corresponding to only one of the nominal polarizations (e.g. , +45°) are simulated and the corresponding field strengths in the vicinity of the base station antenna are calculated. (ii) The power per port, compared with the case when all ports are excited, is doubled. Here it is assumed that the number of ports is the same for each polarization ($\pm 45^\circ$). (iii) The fields are combined using the Magnitude method.

Varying amplitude and phase distributions for a fixed transmitted power. For the case where the excitations may vary both in amplitude and phase for a fixed transmitted power it is possible to analytically determine an optimal set of weight coefficients per assessment point which will maximize the combined field. The combined electric field can be written as

$$E_{\text{rms}}(\mathbf{r}) = \left| \sum_{n=1}^N w_n^{\text{opt}} \mathbf{E}_n(\mathbf{r}) \right|_{\text{rms}} . \quad (\text{Optimal Weights method}) \quad (6)$$

The optimal set of weights $\mathbf{w}^{\text{opt}} = (w_1^{\text{opt}}, \dots, w_N^{\text{opt}})$ can be determined as the eigenvector corresponding to the largest eigenvalue of the $N \times N$ matrix \mathbf{P} with elements (see Appendix)

$$P_{mn}(\mathbf{r}) = \mathbf{E}_m^*(\mathbf{r}) \cdot \mathbf{E}_n(\mathbf{r}) \quad m = 1..N, n = 1..N \quad (7)$$

Product compliance assessments

The most accurate compliance boundary for a given assessment method can be obtained as an iso-surface with its level equal to the reference level or basic restriction. Since this surface is typically quite complex, the iso-surface is often simplified by circumscribing it with a rectangular box or a circular cylinder

[Joseph and Martens, 2005; Thors et al., 2009; CENELEC, 2010]. The price for the gained simplicity is a slightly more conservative compliance boundary. In this work, box-shaped compliance boundaries based on the ICNIRP reference levels and basic restrictions [ICNIRP, 1998] are used. One purpose of this paper is to compare standardized field-based and SAR-based product compliance assessments methods using numerical simulations. The following methods for assessing compliance distances are included in the analysis: (i) Peak root-mean-squared electric and magnetic field strengths compared with the reference levels [CENELEC, 2010; IEC, 2011]. (ii) Peak 10g averaged SAR compared with the basic restrictions [IEC, 2011]. (iii) Root-mean-squared electric and magnetic field strengths averaged over an area of $0.6 \times 0.4 \text{ m}^2$ compared with the reference levels [CENELEC, 2010; IEC, 2011]. (iv) Whole-body averaged SAR compared with the basic restrictions [IEC, 2011]. In this context, the averaged field strengths are used as a proxy for whole-body SAR.

Multi-band base station antenna. In this paper a multiple-frequency or multi-band base station antenna designed for mobile communication is studied. The analysis is based on numerical simulations of a model corresponding to the commercial base station antenna Powerwave P65-15-XDHW2-MD1 (Santa Ana, California), see Table 1. The antenna transmits in four communication bands, which are studied here using the single frequencies of 800, 900, 1800, and 2600 MHz. For this case, all compliance assessment methods described above have been considered and compared in terms of the front compliance distance.

First, the individual frequency bands are treated separately. A transmitted power of $P_n = |w_n|^2$, see Equation (1), for frequency band n will result in an electric field $\mathbf{E}_n(\mathbf{r}, f_n, P_n)$ at the observation point \mathbf{r} . From this vector field, the rms electric field strength averaged over a plane of $0.4 \times 0.6 \text{ m}^2$, centered and placed at a distance d in front of the antenna, $E_{n,\text{rms}}^{\text{av}}(d, f_n, P_n)$, is determined [CENELEC, 2010]. The corresponding peak rms electric field strength, denoted as $E_{n,\text{rms}}^{\text{peak}}(d, f_n, P_n)$, is obtained as the maximum electric field strength within the plane. These rms field strength values are compared with the reference levels [ICNIRP, 1998] to determine front compliance distances $d^{E_{\text{rms}}^{\text{av}}}$ and $d^{E_{\text{rms}}^{\text{peak}}}$ as functions of the transmitted power.

Numerical SAR assessments are conducted by a straightforward extension of the conservative procedure for SAR measurements in the international standard IEC 62232 using a homogeneous box-shaped phantom with dimensions $1.54 \text{ m} \times 0.339 \text{ m} \times 0.15 \text{ m}$ and dielectric parameters corresponding to the tissue-equivalent liquid for the considered frequencies [IEC, 2011]. The dimensions of this phantom were derived to obtain conservative whole-body SAR results for 95% of the adult population [Gosselin et al., 2011]. Also for spatial peak SAR, conservative results are obtained [IEC, 2011]. The density of the phantom is set to 1000 kg/m^3 as specified in IEC 62232. With the phantom centered in front of the antenna, a part of the transmitted power will be absorbed inside it. This absorption is studied using the whole-body averaged SAR (SAR_{wb}) and the peak 10g averaged SAR (SAR_{10g}), which both may be expressed as a function of the phantom-antenna separation distance, d , the frequency, f_n , and the transmitted power, P_n . In order to determine the whole-body averaged SAR, the absorbed power in a sub-volume of the phantom with dimensions $1.54 \times 0.339 \times 0.09 \text{ m}^3$ is determined and divided by a mass of 46 kg for adults and a mass of 12.5 kg for children [IEC, 2011]. Correction factors, to account for the tissue layering effect and varying element load conditions, were also used as required by the procedure in IEC 62232 to obtain conservative results. Similarly to the field-based compliance assessments, the SAR values are compared with the ICNIRP basic restrictions [ICNIRP, 1998] to determine front compliance distances $d^{SAR_{wb}}$ and $d^{SAR_{10g}}$ as functions of the transmitted power.

The discussion above can be generalized to the case where the antenna transmits simultaneously in more than one frequency band. The resulting cumulative compliance distance will depend on how the transmitted power is distributed among the frequency bands. In this study, focus for the combined case is on worst-case cumulative compliance distance providing an upper bound for all excitation combinations. A worst-case \mathbf{w} is therefore determined, which maximizes the ER introduced in Equation (1). A similar approach is adopted for SAR quantities using the basic restrictions instead of the reference levels.

Base station antenna used for MIMO applications. For the MIMO investigation, a multi-column array antenna from Tongyu (TYDA-202415D4T0, Zhongshan City, Guandong, China) with slanted $\pm 45^\circ$ antenna polarization ports (denoted “X-polarized”) is selected. The antenna has four ports per

polarization, i.e., eight ports in total, and the assessments were made for LTE band 39 (1880-1920 MHz). Each port feeds one column containing ten elements of the same nominal polarization (+45° or -45°). In this paper, the following two exposure scenarios are analyzed: (i) four ports of the same nominal polarization excited (denoted “Co-pol case”) and (ii) all eight ports excited (denoted “X-pol case”). The dosimetric quantities considered for the MIMO investigation are the peak rms electric and magnetic field strengths. The goal is to evaluate the different field combining methods for correlated exposure by using Equations (2) – (7) and assess their applicability for the Co-pol and X-pol exposure scenarios mentioned above. The resulting rms field strength values are compared with the reference levels [ICNIRP, 1998] to determine box-shaped compliance boundary dimensions as functions of the total transmitted power.

Numerical simulations

The first challenge, when conducting a numerical product compliance assessment of a base station, is to create a model of the corresponding base station antenna which is meshed according to the numerical algorithm employed. Computer-aided design (CAD) files of the antenna are usually considered as proprietary information by the antenna manufacturer and are therefore seldom available. As a consequence, simplified antenna models have to be created using the modeling tools of the used electromagnetic simulation software. In this work the numerical models were created from physical measurements of real antennas with the antenna radomes removed. The number of antenna elements, polarizations and antenna ground plane dimensions of the models were replicated from the real antennas. For simplicity, the feed networks and the detailed antenna element structures were replaced by arrays of simple wire dipoles fed with voltage sources at the center of each element. This simplification should provide accurate results for SAR simulations when the separation distance between the antenna and the phantom is larger than 1-2 wavelengths [van Wyk et al., 2005; Hansson et al., 2011]. The dimensions of the antenna elements and the reflectors were adapted to obtain a good impedance match and fulfill set tolerance requirements on the vertical and horizontal half-power beam widths (VHPBW and HHPBW). More specifically, the standing wave ratio (SWR) was kept below 2 at the considered frequencies and the VHPBW and HHPBW were within 1° and 5° from the nominal values of the real antennas, respectively.

The simulated electric and magnetic fields were normalized to the power accepted by the antenna ports. For the MIMO array antenna, the tolerance evaluation was conducted for a uniform port excitation, i.e., with the main beam pointing in the broadside direction. A summary of some electrical and mechanical properties of the antennas considered is given in Table 1.

Multi-band base station antenna. For the multi-band antenna, the antenna elements corresponding to the different frequency bands are arranged in an interleaved configuration in front of the ground plane. For the two lowest frequencies, the elements are distributed over the entire length of the ground plane while the dipoles transmitting in the 1800 MHz and 2600 MHz bands are located at the lower and upper part of the antenna array, respectively.

The simulations were conducted using the finite-difference time-domain (FDTD) solver SEMCAD-X version 14.8 by SPEAG (Zürich, Switzerland). The simulation domain was discretized according to the FDTD algorithm using a grid-step smaller than 7% of the considered medium wavelength. Uniaxial perfectly matched layers (UPML) [Gedney, 1996] were used to truncate the simulation domain and to prevent unphysical reflections. At each of the four studied single-frequencies, two types of simulations were carried out: free-space simulations where the electric and magnetic fields in front of the multiband antenna were determined and SAR simulations where the IEC box-shaped phantom was placed in front of the antenna at several separation distances. For antenna-phantom separation distances larger than or equal to 2.5 m, a hybrid configuration called the Generalized Huygens' Box Method (GHBM) is used [Vermeeren et al., 2010; Gosselin et al., 2011; Thielens et al., 2013]. In this method, two separate simulations are required. First, the antenna is simulated in free space, i.e., in absence of the phantom, in order to determine the electric fields over a box-shaped surface which would have surrounded the phantom if it had been present. Secondly, the FDTD algorithm is used to determine the electric fields inside the phantom using the results from the first simulation as excitation. The additional error on the determination of SAR_{wb} and peak SAR_{10g} using this GHBM method, for antenna-phantom separation distances larger than 2 m, is estimated to be around 9% on average for a similar antenna [Thielens et al.,

2013]. This is a small additional error compared to the total worst-case error estimated on compliance distances using the same antenna which is >40% [Thielens et al., 2013].”

Base station antenna used for MIMO applications. For the MIMO investigation, the Method of Moments based solver FEKO version 6.0 by Electromagnetic Software and Systems (EMSS, Stellenbosch, South Africa) is used to simulate electric and magnetic fields in the vicinity of the base station antenna. The distance between the array columns is 0.41 wavelengths at the considered frequency (1880 MHz) which implies that it is important to model the mutual coupling between the antenna elements [Amitay et al., 1972]. At the same time it is desirable to obtain field distributions for each port separately, to be able to investigate the different combination methods. To satisfy both these requirements an embedded pattern approach is used where each port is excited and simulated separately with the other ports terminated in matched loads [Bhattacharyya, 2006]. The triangle edge length and the wire segment length in the FEKO model are kept below 1/16 and 1/20 of the wavelength, respectively [EMSS, 2010].

Reference measurements

Reference results are obtained based on full-sphere far-field measurements of the considered base station antenna used for the MIMO investigation. The embedded far-field patterns are measured per port and frequency band considered. Subsequently, the measured far-fields are expanded in spherical vector waves and back-propagated to the near-field to allow comparisons with simulated results [Fridén, 2003].

RESULTS

Compliance boundaries of multi-band base station antenna

Figure 1 shows the obtained compliance boundaries and the corresponding maximum allowed output powers in front of the multi-band base station antenna using single-band transmission. Compliance distances for different methods and frequencies are shown versus phantom-antenna separation distance. The black and blue curves indicate the compliance distances based on whole-body averaged SAR and peak 10g averaged SAR for head and trunk exposure [ICNIRP, 1998], using the scale factors and phantom described in IEC 62232 [IEC, 2011]. The SAR_{wb} is calculated using masses of 46 kg (black

dashed curve) and 12.5 kg (blue dashed curve), corresponding to an adult and a child, respectively [IEC, 2011]. The red curves indicate the compliance distances, based on the electric and magnetic field strengths averaged over a centered surface of $0.4 \times 0.6 \text{ m}^2$ [CENELEC, 2010] and the corresponding maximal rms value of the fields in that plane. The electric field was found to always produce a larger compliance distance than the magnetic field. The results in Figures 1 and 2 correspond to the electric field.

The maximum allowed output powers based on the peak 10g-averaged SAR, $P_{\text{compl}}^{\text{SAR}_{10\text{g}}}$, are in very good agreement with those found in Thielens et al. [2013] for the peak 10g SAR in the head and trunk of the Virtual Family male [Christ et al., 2010] under exposure from a similar antenna with the same number of radiating elements (except at 2600 MHz), antenna area, element spacing, and HPBW. The modeling approach in the two studies are slightly different: in this study the antenna is modeled as a simple dipole array, while in Thielens et al. [2013] the antenna structure is fully modeled.

Figure 2 shows the worst-case combined compliance distances based on the exposure assessment quantities considered in this paper.

Compliance boundaries of base station antenna used for MIMO applications

In the following subsections, compliance boundary results are presented for the different exposure configurations and field combining methods investigated. All field computations are made in three-dimensional volumes and the compliance boundaries are determined based on 3D data. Results on the compliance boundary heights are deliberately excluded since the different methods investigated were found to produce very similar results.

Reference measurements. A comparison between simulations and measurements, in terms of compliance boundary dimensions and combined electric field distributions in a vertically centered horizontal plane, is shown in Figure 3 for the Tongyu antenna with four ports excited uniformly corresponding to a nominal polarization of $+45^\circ$ (Co-pol case). The total transmitted power is 49.5 dBm (89.1 W) and the Magnitude method in Equation (2) is used to combine the fields. The solid and dashed

yellow lines correspond to the horizontal compliance boundary based on ICNIRP's reference levels [ICNIRP, 1998] for general public and occupational exposure, respectively. As shown in Figure 3, the overall agreement in terms of the field pattern shape is very good. The measured far-field cannot be accurately back-propagated into the reactive near-field region [Fridén, 2003]. Data is therefore not available in the immediate vicinity of the base station antenna which explains the white circle in Figure 3b. For power levels between 10 W to 100 W, the maximum discrepancy in front compliance distance between the measured and simulated results is 8 % (not shown). This confirms the quality and reliability of the used numerical antenna models.

MIMO array analysis, co-pol case. In this section, results from the MIMO co-pol array analysis are given. For the cases where the amplitude distribution is fixed, see Equations (2)-(4), a uniform amplitude distribution is used.

First, an analysis on the number of random phases needed to obtain convergence in compliance boundary dimensions using Equation (4) is conducted. It is found that with the used sampling interval of 0.1 m, the Random Phase method is quite robust also for a low number of random phases. For the investigated configuration, three random phases per port are needed to obtain front compliance distances within 0.1 m from the converged values (obtained for $N_p = 8$). In Figure 4, the combined electric field distribution in a vertically centered horizontal plane, and the resulting compliance boundary dimensions, are shown for the co-pol case and a total transmitted power of 49.5 dBm (89.1 W) using the Random Phase method with $N_p = 4$. The obtained front compliance distances for general public and occupational exposure were 11.1 m and 4.7 m, respectively. The fragmented contour plot is a consequence of the randomly selected phase angles.

Compliance boundary dimensions for different field combining methods and the co-pol case are compared in the upper part of Table 2. The Components and Magnitude methods produce essentially the same front compliance distance as the Random Phase method (deviation $\Delta \leq 1\%$). For the compliance boundary width, the corresponding deviation was less than 2.4%. Similar results are also obtained for the Optimal Weights method, see Table 2. As expected, the compliance boundary dimensions are always

larger for the Optimal Weights method compared with the Random Phase method. For the co-pol case, and using a dedicated computer with no other computationally intensive processes running, the Magnitude method was found to be about 10 to 100 times faster than the Optimal Weights and the Random Phase ($N_p = 3$) methods, respectively.

MIMO array analysis, X-pol case. .

In the lower part of Table 2, the X-pol Magnitude method is compared against the Random Phase method with $N_p = 3$. Note that for the Random Phase method ports with both polarizations are considered, while the X-pol Magnitude method only uses simulations of one polarization. The proposed X-pol magnitude method is shown to produce conservative results with a maximum deviation in front compliance distance of +3.3% obtained for a transmitted power of 20 W. The front compliance distance obtained using the Random Phase method was 4.8 m for this case. For the compliance boundary width, the corresponding maximum deviation is +5.0%. For this case, the X-pol Magnitude method was found to be about 1000 times faster than the Random Phase method.

DISCUSSION

Compliance assessments of multi-band base station antennas

Compliance distances have been determined based on the ICNIRP reference levels and basic restrictions for a multi-band base station antenna, to evaluate the procedures described in CENELEC European standard (EN) 50383 [CENELEC, 2010] and IEC 62232 [IEC, 2011]. The goal is to determine a total compliance distance, d_{tot} , at which the exposure is below relevant limits on both localized and whole-body exposure. Using the notation employed before, the total compliance distance can be determined using any of the approaches listed below in order of increasing computational demands

$$d_{\text{tot}} = \max(d^{E_{\text{rms}}^{\text{av}}}, d^{E_{\text{rms}}^{\text{peak}}}) = d^{E_{\text{rms}}^{\text{peak}}} \quad (8)$$

$$d_{\text{tot}} = \max(d^{E_{\text{rms}}^{\text{av}}}, d^{SAR_{10g}}) \quad (9)$$

$$d_{\text{tot}} = \max(d^{SAR_{\text{wb}}}, d^{SAR_{10g}}) \quad (10)$$

Only one simulation is required to obtain field strength results for all investigated assessment distances. For SAR, however, one simulation is needed per assessment point. Furthermore, the SAR simulations normally make use of more mesh cells in order to discretize the phantom due to the shorter medium wavelength. If the assessments are made using Equation (9), i.e., the SAR assessment is made with respect to localized SAR only, the assessments may be simplified compared with Equation (10) by using an elliptical phantom, significantly smaller than the box-shaped phantom required to assess whole-body SAR [IEC, 2011]. The major and minor axes of the specified ellipse are 0.60 m and 0.40 m, respectively, which may be compared with the lateral dimensions of the box-shaped phantom of 1.54 m and 0.34 m.

As expected, Figure 1 shows that the simplest approach for assessing EMF compliance, i.e., E_{rms}^{peak} field assessment by using Equation (8), will provide the most conservative compliance boundary results for adult exposure. For a given power level, the front compliance distance may be reduced significantly if the assessments instead are conducted according to Equation (9). As an example, for a transmit power of 10 W at 900 MHz, the compliance distance is reduced from about 2 m to 1.5 m if a combination of averaged field strengths and peak 10g SAR is used. For pure SAR-based assessments, using Equation (10), even smaller compliance distances are obtained for the two lower frequencies, while for the two higher frequencies, Equations (9) and (10) are found to produce very similar results. The obtained frequency dependence may partly be attributed to the frequency dependent reference levels and partly to the distribution of the antenna elements. For the cumulative exposure, it is found that Equation (8) will provide the largest compliance distance and Equation (10) will give the shortest compliance distance.

An interesting question is to what extent these results may be generalized to other antennas. The most conservative compliance distance is likely to be obtained for peak field strength assessments due to the definition of ICNIRP's reference levels [ICNIRP, 1998]. When it comes to spatial field averaging and whole-body SAR, key factors to consider are the sizes of the averaging surface and the phantom compared with the incident field spatial distribution. The extent of the incident field spatial distribution will in turn depend on the size of the antenna and the distance from the antenna to the assessment point.

As a consequence, it is not possible to generalize the results above in a broad sense. For base station antennas similar to the ones investigated, however, the results should be representative.

When child exposure is considered, Figure 1 shows that there exist power levels for which Equation (10) will predict a larger compliance distance than Equation (8). This is partly a consequence of the very conservative approach specified in IEC 62232, where the whole-body SAR is obtained as the power absorbed in an adult phantom divided by the mass of a child.

By assuming that all power transmitted by the antenna is absorbed in the phantom, a theoretical lower limit in transmitted power (P_{lim}) that can result in a whole-body SAR equal to the ICNIRP basic restriction can be calculated as the product of the basic restriction on SAR_{wb} and the mass of the phantom.

For the adult phantom $P_{lim} = 0.08 \frac{W}{kg} \cdot 46 \text{ kg} = 3.68 \text{ W}$, while for the child phantom $P_{lim} = 1 \text{ W}$. As shown in Figure 1, the whole-body SAR approach of IEC 62232 may for small phantom-antenna separation distances produce even lower maximum allowed power levels. This unphysical behavior is a consequence of the distance independent tissue layering correction factor specified in IEC 62232 [IEC, 2011]. These results are consistent with the results obtained in [Thors et al., 2013] where a distance dependent correction factor is proposed.

The whole-body SAR values determined for the adult phantom in this study are about a factor of 2 higher than those in Thielens et al. [2013], which was to be expected since, as mentioned in the Materials and Method section, the IEC phantom is designed to have a SAR higher than 95% of the SARs found in realistic phantoms [Gosselin et al., 2011].

Base station antenna used for MIMO applications

For the co-pol case, four different field combining methods were investigated. In situations where both the amplitude and the phase of the excitation may vary, the Optimal Weights method provides an upper bound of the combined field strengths levels. For situations where the excitation amplitudes are fixed but the phases may vary, the Random Phase method may be used to obtain a best estimate of the compliance boundary dimensions. This is because the basis of the Random Phase method consists of determining the

combined field strength levels for specific phase excitations by summing the individual contributions to amplitude and phase and then retaining the maximum value obtained. If enough random samples are selected to reach convergence in terms of compliance boundary dimensions a best estimate for the considered exposure configuration is obtained. The drawback of this method is its high computational requirements. Another option is therefore to use the conservative Magnitude or Components methods, which for the co-pol case is found to result in very small overestimations of the compliance boundary dimensions. The overestimation in front compliance distance, compared with the Random Phase method, is found to be 1% or less as a consequence of the uniform polarization in the main beam direction. For the compliance boundary width, the corresponding maximum overestimation is found to be 2.4%. The largest deviations for the Magnitude methods in terms of combined field strength levels are found at points interior to the compliance boundary, where fields from different antenna elements have a comparable magnitude but different polarizations. These points are, for practical macro RBS power levels, not relevant for compliance boundary assessments.

A comparison of the required simulation times will depend on different parameters such as the number of sources, the spatial assessment point density, and the number of random phases. For the Co-pol case considered, with 4 sources, a sampling interval of 0.1 m, and $N_p = 3$, the Magnitude method is found to be about 100 times faster than the Random Phase method. Due to its computational efficiency and the small overestimation introduced, the Magnitude method is very attractive for determining compliance boundaries of antennas with co-polarized elements. Compared with the other methods, another advantage of the Magnitude method is that only the field magnitudes need to be stored which will reduce the memory requirements correspondingly.

The Optimal Weights method gives a larger front compliance distance compared with the Magnitude method. The explanation for this is that the vector fields corresponding to the individual ports are aligned in the front direction. Hence, the Magnitude method does not add anything to the total field magnitude whereas the Optimal Weights method can reach a larger field magnitude by redistributing the powers transmitted by the antenna ports. Note that the latter effect is small in the main lobe. This alignment of

field vectors is not necessarily obtained in other field evaluation points, depending on effects of mutual coupling and chosen antenna element. As a consequence, for the studied antenna the widest compliance boundary is instead obtained for the Magnitude method.

It is found that the proposed X-pol Magnitude method results in conservative compliance distances compared with the reference Random phase method, with maximum deviations of 3.3% and 5.0% for the front compliance distance and the compliance boundary width, respectively. Advantages of this approach are that the simulation time decreases significantly (about a factor of 1000 for $N_p = 3$ and a sampling interval of 0.1 m) and only ports corresponding to one of the antenna polarizations need to be modeled.

By comparing the results obtained for the Co-pol and X-pol assessments it is clear that smaller compliance boundaries are obtained for the X-pol case since the available power is distributed over the two polarizations. As an example, for a transmitted power of 40 W and frequency 1800 MHz, the front compliance distances are 7.3 m and 7.1 m for the Co-pol and X-pol cases, respectively.

As shown in Figure 3, lower field strength levels are obtained for the measurements in comparison with the simulations, resulting in a front compliance distance reduction of 7% (0.8 m) for general public exposure. This may be explained by a somewhat lower realized gain for the real antenna due to losses, which are not included in the numerical model.

CONCLUSIONS

In this paper, various aspects of numerical RF exposure compliance assessments of mobile communication radio base station products are investigated. Different standardized assessment methods, for comparison with the ICNIRP reference levels and basic restrictions are evaluated in terms of resulting compliance distances for a multi-band base station antenna and a base station antenna employing MIMO transmission schemes. Both frequency specific and cumulative compliance distances, based on different quantities such as peak 10g averaged specific absorption rate (SAR), whole-body averaged SAR, and peak and spatially averaged root-mean-squared electric and magnetic fields, are determined. Moreover,

the gain, in terms of accurate compliance distances when using more laborious assessment methods, is quantified.

In general, assessments based on peak field strengths are less computationally intensive but lead to larger compliance distances. As expected, it is found that spatial field averaging used in combination with localized SAR assessments is an option to obtain shorter compliance distances. As long as adult exposure is considered, the results also indicate that even shorter compliance distances may be obtained by using assessments based on localized and whole-body SAR. The currently specified procedure in IEC 62232 for evaluating child whole-body SAR, results in compliance distances larger than the peak field strength method for some scenarios. It is also shown that the currently standardized whole-body SAR measurement approach in IEC 62232 may lead to unphysical results for small phantom-antenna separation distances.

Multiport base station arrays with densely spaced columns are investigated to determine procedures suitable for numerical compliance assessments of radio base station products employing MIMO transmission schemes. For efficient assessments, a distinction is made between methods where the amplitude distribution is fixed and methods for which both the amplitude and phase may vary. For the latter case, a field combining method denoted Optimal Weights is proposed which is found to provide an upper bound of the combined field strengths levels. For transmission schemes where the amplitude distribution is fixed, a field combining method, based on evaluation of a number of random phase distributions per field evaluation point, is proposed as a best estimate method. For the case when all considered ports have the same nominal polarization, the Magnitude method is found to produce only a minor over-estimation of the compliance boundary dimensions. Due to its efficiency compared with the best estimate method, the Magnitude field combining approach is recommended for this case. For cases where the considered ports have different antenna polarizations, an efficient procedure based on simulations of only one of the antenna polarizations is proposed.

The results presented in this study can be used by manufacturers of radio base station products or their clients who need to efficiently determine compliance with exposure limits or regulations. For the

multiband base station antenna case, this study will be extended to other directions using surrogate modeling to reduce the number of computationally expensive SAR simulations. For MIMO antennas an interesting extension is the assessment of exposure of large multi-port array antennas.

REFERENCES

- Amitay N, Galindo V, Wu CP. 1972. Theory and Analysis of Phased Array Antennas. New York, Wiley-Interscience.
- Balanis A. 2005. Antenna Theory: Analysis and Design. 3rd edition. Hoboken, Wiley & Sons.
- Bhattacharyya. 2006. Phased array antennas: Floquet analysis, Synthesis, BFNs, and active arrays systems. Hoboken, NJ, Wiley-Interscience.
- CENELEC 2010. Basic standard for the calculation and measurement of electromagnetic field strength and SAR related to human exposure from radio base stations and fixed terminal stations for wireless telecommunication systems (110 MHz – 40 GHz). CENELEC EN 50383:2010, Brussels, Belgium.
- Christ A, Kainz W, Hahn EG, Honegger K, Zefferer M, Neufeld E, Rascher W, Janka R, Bautz W, Chen J, Kiefer B, Schmitt P, Hollenbach H, Shen J, Oberle M, Szczerba D, Kam A, Guag JW, Kuster N. 2010. The Virtual Family-Development of surface-based anatomical models of two adults and two children for dosimetric simulations. *Phys Med Biol* 55:N23–N38.
- Cooper J, Marx B, Buhl J, Hombach V. 2002. Determination of safety distance limits for a human near a cellular base station antenna, adopting the IEEE standard or ICNIRP guidelines. *Bioelectromagnetics* 23:429-443.
- Dahlman E, Parkvall S, Sköld J, Beming P. 2008. 3G Evolution: HSPA and LTE for Mobile Broadband. 2nd edition. Oxford, UK: Academic Press.
- Dimbylow PJ. 2002. Fine resolution calculations of SAR in the human body for frequencies up to 3 GHz. *Phys Med Biol* 47:2835-2846.
- EMSS. 2010. FEKO user's manual., Stellenbosch, South Africa, Available from: <http://www.feko.info/download> (license required, Last accessed 3 September, 2013).

- Fridén J. 2003. RF exposure compliance boundary analysis of base station antennas using combined spherical-cylindrical near-field transformations. *Electron Lett* 39:1783-1784.
- Gedney SD. 1996. An anisotropic perfectly matched layer absorbing media for the truncation of FDTD lattices. *IEEE Trans Antennas Propag* 44:1630–163.
- Gosselin MC, Vermeeren G, Kuhn S, Kellerman V, Benkler S, Uusitupa TMI, Joseph W, Gati A, Wiart J, Meyer FJC, Martens L, Nojima T, Hikage T, Balzano Q, Christ A, Kuster N. 2011. Estimation formulas for the specific absorption rate in humans exposed to base-station antennas. *IEEE Trans Electromagn Compat* 53(4):909–922.
- Hansson B, Thors B, Törnevik C. 2011. Analysis of the effect of mobile phone base station antenna loading on localized SAR and its consequences for measurements. *Bioelectromagnetics* 32:664-672.
- ICNIRP 1998. Guidelines for limiting exposure to time-varying electric, magnetic, and electro-magnetic fields (up to 300 GHz). *Health Physics* 74:494-522.
- IEC 2010. Guidance for evaluating exposure from multiple EM sources. IEC 62630:2010, Geneva, Switzerland.
- IEC 2011. Determination of RF fields in the vicinity of mobile communication base stations for the purpose of evaluating human exposure. IEC 62232:2011, Geneva, Switzerland.
- Joseph W, Verloock L, Martens L. 2003. Accurate low-cost measurement technique for occupational exposure assessment of base station antennas. *Electron Lett* 39:886-887.
- Joseph W, Martens L. 2005. Comparison of safety distances based on the electromagnetic field and based on the SAR for occupational exposure of a 900-MHz Base station antenna. *IEEE Trans Electromagn Compat* 47:977-985.
- Kos B, Valič B, Kotnik T, Gajšek, P. 2011. Exposure assessment in front of a multi-band base station antenna. *Bioelectromagnetics* 32:234-242.
- Lacroux F, Conil E, Carrasco A, Gati A, Wong MF, Wiart J. 2008. Specific absorption rate assessment near a base station antenna (2,140 MHz): some key points. *Ann Telecommun*, 63:55–64.

- Martínez-Búrdalo M, Martín A, Anguiano M, Villar R. 2005. On the safety assessment of human exposure in the proximity of cellular communications base-station antennas at 900, 1800 and 2170 MHz, *Phys Med Biol* 50:4125-4137.
- Perentos N, Iskra S, Faraone A, McKenzie RJ, Bit-Babik G, Anderson V. 2012. Exposure Compliance Methodologies for Multiple Input Multiple Output (MIMO) Enabled Networks and Terminals, *IEEE Trans Antennas Propag* 60:644-653.
- Thielens A, Vermeeren G, Kurup D, Joseph W, Martens L. 2013. Compliance Boundaries for Multiple-Frequency Base Station Antennas in Three Directions. *Bioelectromagnetics* 34:465-478.
- Thors B, Hansson B, Törnevik C. 2009. The generation of simple compliance boundaries for mobile communication base station antennas using formulae for SAR estimation. *Phys Med Biol*, 54:4243-4256.
- Thors B, Nord L, Colombi D, Törnevik C. 2013. Product compliance assessments of low power radio base stations with respect to whole-body radiofrequency exposure limits. *Antennas and Propagation (EuCAP), 2013 7th European Conference on*, Gothenburg, Sweden.
- Van Wyk M, Bingle M, Meyer FJC. 2005. Antenna modeling considerations for accurate SAR calculations in human phantoms in close proximity to GSM cellular base station antennas. *Bioelectromagnetics* 26:502-509.
- Vermeeren G, Gosselin MC, Kuhn S, Kellerman V, Hadjem A, Gati A, Joseph W, Wiart J, Meyer F, Kuster N, Martens L. 2010. Influence of the reflective environment on the absorption of a human male exposed to representative base station antennas from 300 MHz to 5 GHz. *Phys Med Biol* 55(18):5541–5555.

APPENDIX

The combined electric field from N antennas operating at the same frequency can at some point in space be written as

$$\mathbf{E}(\mathbf{r}) = \sum_{n=1}^N w_n \mathbf{E}_n(\mathbf{r}) \quad (A-1)$$

where w_n and $\mathbf{E}_n(\mathbf{r})$ denote the complex excitation coefficients associated with port n and the corresponding electric field strengths for a unitary excitation ($\forall i = 1..N: w_i = \delta_{in}$), respectively. The scope of the analysis is to determine a set of weights w_n which maximizes the expression (\mathbf{r} is omitted in the following equations):

$$p(\mathbf{w}) = \mathbf{E}^* \cdot \mathbf{E} = \sum_{m=1}^N \sum_{n=1}^N w_m^* \mathbf{E}_m^* \cdot w_n \mathbf{E}_n = \mathbf{w}^H \mathbf{P} \mathbf{w}, \quad (A-2)$$

where \mathbf{w} denotes the weight vector and the matrix elements of the Hermitian matrix \mathbf{P} are given by

$$P_{mn} = \mathbf{E}_m^* \cdot \mathbf{E}_n. \quad (A-3)$$

The total transmitted power is denoted P_{tot} , i.e., $\mathbf{w}^H \mathbf{w} = P_{\text{tot}}$. The maximum value of $\mathbf{w}^H \mathbf{P} \mathbf{w}$ is obtained when \mathbf{w} is the eigenvector corresponding to the largest eigenvalue of \mathbf{P} . The corresponding maximum value can therefore be written as $\max(\mathbf{w}^H \mathbf{P} \mathbf{w}) = \max_i(\lambda_i) P_{\text{tot}}$ where λ_i are the eigenvalues of \mathbf{P} . A similar approach can of course also be used for the magnetic field.

Figure captions

Fig. 1. Compliance distances for the studied multiband antenna based on the ICNIRP basic restrictions using the IEC box phantom [IEC, 2011] and reference levels for the electric field averaged over the CENELEC plane [CENELEC, 2010] and the maximum in that plane (a) 800 MHz (b) 900 MHz (c) 1800 MHz and (d) 2600 MHz.

Fig. 2. Compliance distances for the studied multiband antenna based on the ICNIRP basic restrictions using the IEC box phantom [IEC, 2011] and reference levels for the electric field averaged over the CENELEC plane [CENELEC, 2010] and the maximum in that plane for cumulative exposure.

Fig. 3. Combined electric field strength levels in a horizontal plane, vertically centered with respect to the transmitting antenna. The Magnitude field combining method was used for a total transmitted power of 49.5 dBm (89.1 W) (co-pol case). The solid and dashed yellow lines correspond to the horizontal compliance boundary based on 3D data for general public and occupational exposure, respectively. (A) Numerical simulations. (B) Measurements.

Fig. 4. Combined electric field strength levels in a horizontal plane, vertically centered with respect to the transmitting antenna, and resulting compliance boundary dimensions based on 3D data. The Random Phase field combining method with four random phases per port and field assessment point was used for a total transmitted power of 49.5 dBm (89.1 W) (co-pol case).

Table Captions

Table 1. Electrical and mechanical properties of the considered antennas.

Table 2. Simulated compliance distances for the general public for different modeling techniques, exposure configurations, and field combination methods.

TABLE 1. Electrical and mechanical properties of the considered antennas

Antenna model	Tested frequency (MHz)	Polarization	Number of antenna elements	Antenna Length/Width/Height (m)	Horizontal / Vertical half-power beam width* (degrees)	Gain (dBi)
Powerwave P65-15-XDHW2-MD1	800	$\pm 45^\circ$	5	1.3 / 0.258 / 0.107	74.8/15.2	14.7
	900	$\pm 45^\circ$	5		71.8/13.7	15.2
	1800	$\pm 45^\circ$	3		72.3/12.6	12.8
	2600	$\pm 45^\circ$	5		58.6/11.4	12.0
Tongyu TYDA 202415D4T0	1880	$\pm 45^\circ$	40 per polarization	1.360 / 0.290 / 0.105	29 / ≥ 7	20

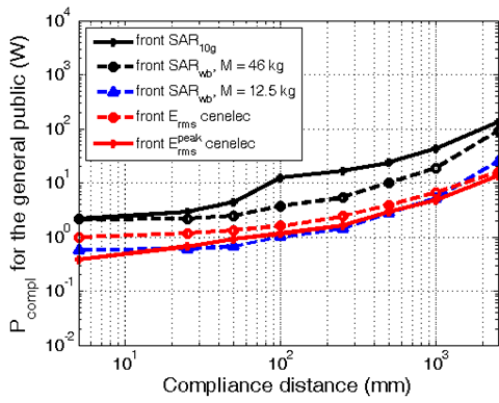
*The gain and half-power beam width values for the Tongyu antenna are with the beam scanned towards broadside.

TABLE 2. Simulated compliance distances for the general public for different modeling techniques, exposure configurations, and field combination methods.

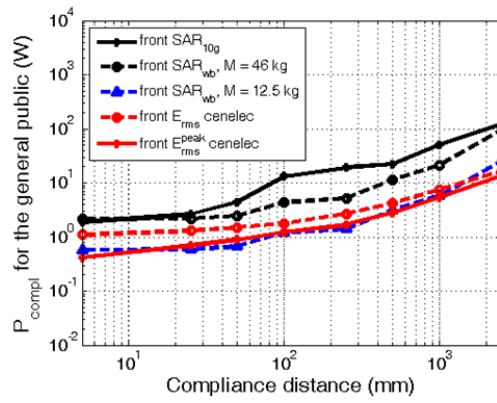
	CB dim.	Method	Compliance distance (m) or Deviation (Δ) from reference results (indicated by [ref.]) (%)				
			P = 20 W	P = 40 W	P = 60 W	P = 80 W	P = 100 W
Co-pol method comparison results	Front	Random Phase [ref.]	4.9 m	7.3 m	9.1 m	10.5 m	11.8 m
	Front	Δ Components	+0.8%	+1.0%	+0.4%	+0.7%	+0.5%
	Front	Δ Magnitude	+0.8%	+1.0%	+0.4%	+0.7%	+0.5%
	Front	Δ Optimal Weights	+0.9%	+1.1%	+0.5%	+0.8%	+0.5%
	Width	Random Phase [ref.]	5.2 m	8.2 m	10.4 m	12.2 m	13.7 m
	Width	Δ Components	+2.2%	+2.1%	+1.5%	+1.5%	+2.0%
	Width	Δ Magnitude	+2.4%	+2.3%	+1.7%	+1.7%	+2.2%
	Width	Δ Optimal Weights	+2.1%	+1.8%	+1.2%	+1.1%	+1.7%
X-pol method comp. res.	Front	Random Phase [ref.]	4.8 m	7.1 m	8.9 m	10.3 m	11.6 m
	Front	Δ X-pol Magnitude	+3.3%	+2.9%	+2.8%	+2.8%	+2.7%
	Width	Random Phase [ref.]	5.1 m	8.0 m	10.1 m	12.0 m	13.5 m
	Width	Δ X-pol Magnitude	+5.0%	+4.9%	+4.8%	+3.3%	+4.0%

*X-pol = all eight ports excited; Co-pol = four ports of the same nominal polarization excited; Magnitude = field combining using the Magnitude method in (3); Components = field combining using the Components method in (4); Random phase = field combining using the Random Phase method in (5); Optimal Weights = field combining using the Optimal Weights method in (7); X-pol Magnitude = field combining using the X-pol Magnitude field combining method.

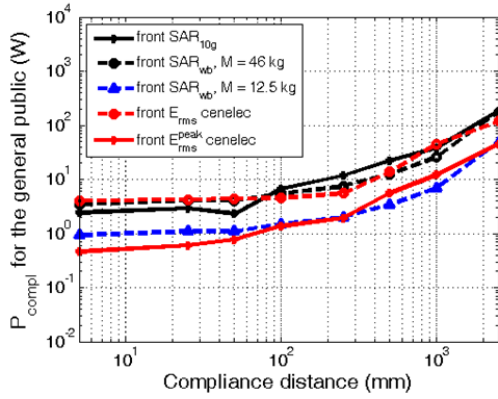
Figures



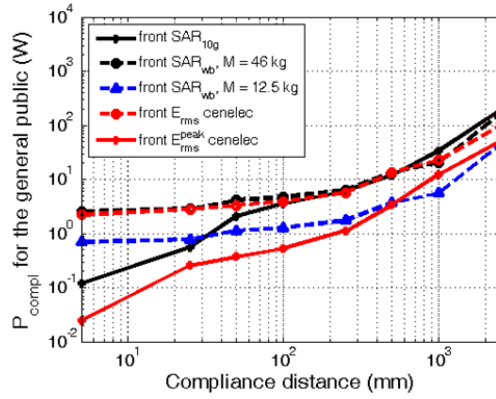
(a)



(b)



(c)



(d)

Fig. 1. Compliance distances for the studied multiband antenna based on the ICNIRP basic restrictions using the IEC box phantom [IEC, 2011] and reference levels for the electric field averaged over the CENELEC plane [CENELEC, 2010] and the maximum in that plane (a) 800 MHz (b) 900 MHz (c) 1800 MHz and (d) 2600 MHz.

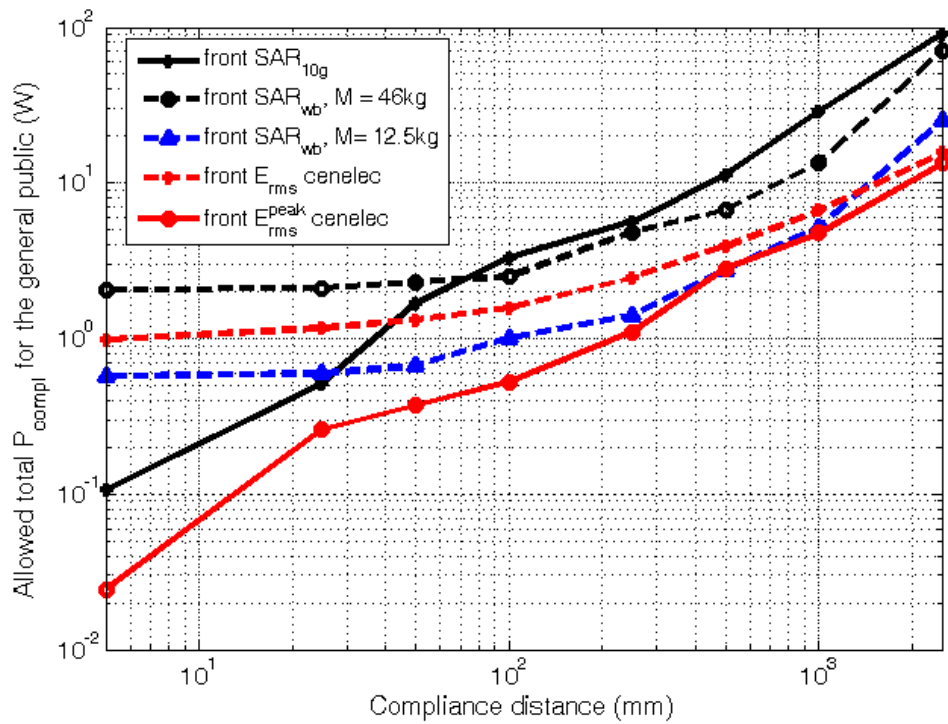


Fig. 2. Compliance distances for the studied multiband antenna based on the ICNIRP basic restrictions using the IEC box phantom [IEC, 2011] and reference levels for the electric field averaged over the CENELEC plane [CENELEC, 2010] and the maximum in that plane for cumulative exposure.

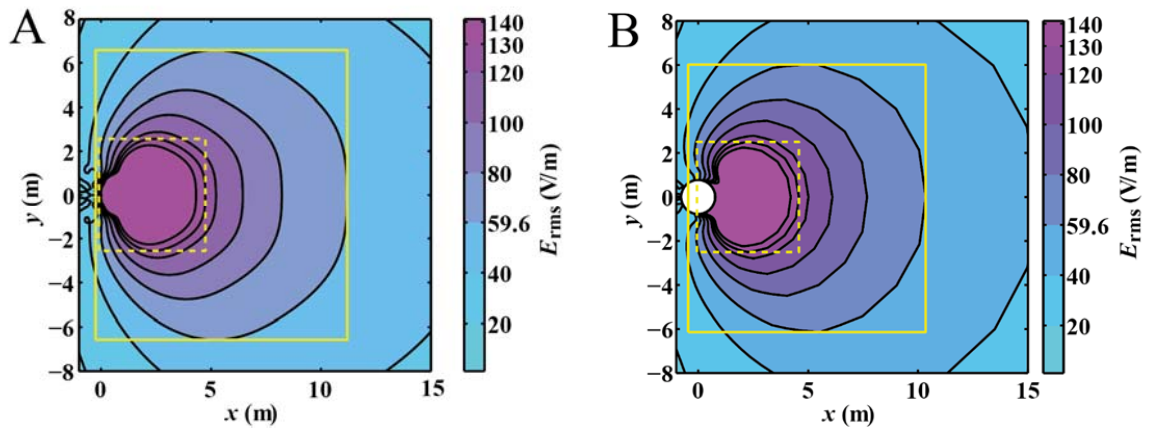


Fig. 3. Combined electric field strength levels in a horizontal plane, vertically centered with respect to the transmitting antenna. The Magnitude field combining method was used for a total transmitted power of 49.5 dBm (89.1 W) (co-pol case). The solid and dashed yellow lines correspond to the horizontal compliance boundary based on 3D data for general public and occupational exposure, respectively. (A) Numerical simulations. (B) Measurements.

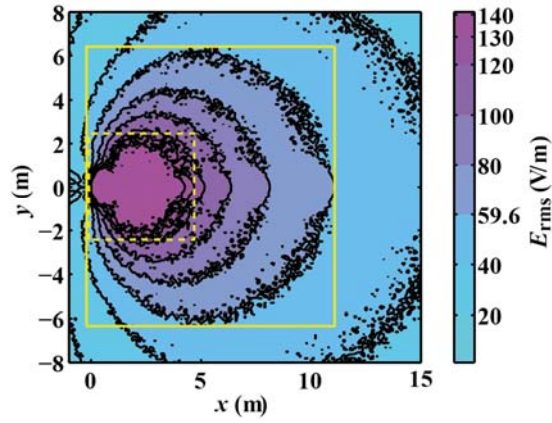


Fig. 4. Combined electric field strength levels in a horizontal plane, vertically centered with respect to the transmitting antenna, and resulting compliance boundary dimensions based on 3D data. The Random Phase field combining method with four random phases per port and field assessment point was used for a total transmitted power of 49.5 dBm (89.1 W) (co-pol case).